Lifting Surface Calculations in the Laplace Domain with Application to Root Loci

Tetsuhiko Ueda*
National Aerospace Laboratory, Chofu, Japan

A method for determining the unsteady aerodynamic forces on a subsonic thin finite wing is presented. The unsteady forces are numerically evaluated as functions of the Laplace transform variable s, which corresponds to both the arbitrary and harmonic motions of a wing. Computation is possible on the entire s plane except for a branch cut on the negative real axis. The method proposed is based on the doublet-point method such that the wing planform may be arbitrary (including the partial control surfaces). The exact forces obtained for the Laplace variable are applied to determine the root loci of a wind tunnel wing model. Comparison of the results with those from the finite-state aerodynamic modeling shows the accuracy of Roger's approximation. The effect of compressibility is also examined to reveal that an aerodynamic root does exist in the range of high subsonic flow.

Nomenclature

a = parameter in Eq. (26)
A = matrix defined by Eq. (16)
b = semichord length of the wing root
B = integral function
D = aerodynamic compliance matrix
h = deflection mode
i = imaginary unit or dummy index
k = reduced frequency
K = kernel function
L = Laplace transform
M = Mach number
N = total number of aerodynamic elements
N^A = total degrees of freedom
p = nondimensional Laplace transform variable
Δp = nondimensional lift distribution
q_i = generalized coordinates
q_{ij} = generalized aerodynamic forces
Q_i = generalized forces
r = nondimensional spanwise distance
R = nondimensional distance parameter defined by Eq. (3b)
s = Laplace transform variable
t = time
U = uniform flow speed
w = nondimensional upwash distribution
x = nondimensional streamwise coordinate based on b
X = nondimensional parameter defined by Eq. (3a)
y = nondimensional spanwise coordinate based on b
β = compressibility parameter
δ = Kronecker delta
Δ_i = nondimensional element area
ϵ = error bound
ξ = dummy streamwise variable
η = dummy spanwise variable
ϕ = deficiency function
κ = eigenvalue
λ = nondimensional parameter defined by Eq. (3f)
ρ = air density
σ = half-width of wing element
ω_i = natural frequency
τ = nondimensional time
ζ_i = damping coefficient

Superscript

$(\bar{\ })$ = Laplace transformed

Received April 23, 1986, presented as Paper 86-0866 at the AIAA/ASME/ASCE/AHS 27th Structures, Structural Dynamics and Materials Conference, San Antonio, TX, May 19-21, 1986; revision received Sept. 24, 1986. Copyright © 1986 by T. Ueda. Published by the American Institute of Aeronautics and Astronautics, Inc. with permission.

* Senior Researcher. Member AIAA.

Introduction

THE recent advent of active control technology (ACT) for large flexible aircraft has renewed interest in the unsteady aerodynamic forces given in the Laplace domain, i.e., the forces as functions of the Laplace transform variable s. In designing control laws for aeroelastic active controls, say, gust load alleviation and/or flutter suppression, an aerodynamically accurate prescription may be an essential part of the system.[1] Especially, aerodynamic effects of control surfaces should be properly included in the analytical model of the system. Two types of approximation have been feasible hitherto for constructing aerodynamical models, i.e., aerodynamic transfer functions. One[2,3] utilizes the forces obtained in the frequency domain that have been intensively investigated by flutter analysts for more than three decades. The harmonic unsteady forces can be interpreted as the forces on the imaginary axis in the complex s plane. Therefore, we can determine coefficients of the aerodynamic transfer functions so that the approximation curve may fit best on the imaginary axis. Although the generalization of the harmonic forces to arbitrary motion (off-axis) gave rise to historical arguments on the validity of the results in the left half-plane, it has been resolved as valid by analytic continuation.[4] The frequency domain approach yields a useful approximation, but is limited to the proximity of the imaginary axis. The other approach[5,6] curve fits the time history data of an aerodynamic response with a certain type of function whose Laplace transform is analytically known. Stark[6] has proposed an accurate time function for a finite wing in incompressible flow. He hypothesized that the normalized deficiency function of the indicial response is independent of the deflection mode of the wing in incompressible flow. He proposed particular deficiency functions for both the subsonic and supersonic flow cases.

For a *subsonic finite* wing, however, there is no rigorous method to clarify the characteristics of the aerodynamic forces off-axis in the left half of the s plane. Hence, the purpose of the present study.

In this paper, a direct method to calculate the Laplace-transformed pressure distributions on subsonic lifting surfaces is developed. The method generalizes the doublet-point method (DMP)[7] of the frequency domain. It can be applied to wings of arbitrary planform. Furthermore, the method is exact in the sense that no approximation is made on the procedure of obtaining the Laplace transform, in contrast with those using the forces in the frequency domain or the time domain responses. As an application of these exact forces in the Laplace domain, root loci are calculated for a wind tunnel wing model that assumes an energy-efficient future transport.

Integral Equation and Solution Method

In the Laplace domain, the objective equation that relates the upwash distributions on a thin finite wing can be written in a similar form to that in the frequency domain,

$$\bar{w}(x,y)=\frac{1}{8\pi}\int\int_{\text{wing}}\Delta\bar{p}(\xi,\eta)\,K(x_0,y_0)\,d\xi\,d\eta \tag{1}$$

where $\bar{w}$ and $\Delta\bar{p}$ are the upwash and pressure distributions, respectively. The singular kernel K in Eq. (1) is given by[8]

$$K(x_0,y_0)=\frac{M^2e^{-p\lambda}}{R\lambda}+e^{-px_0}B(p,r,X) \tag{2}$$

where

$$X=\beta^{-2}(x_0-MR) \tag{3a}$$

$$R=\left(x_0^2+\beta^2r^2\right)^{1/2} \tag{3b}$$

$$r=|y_0| \tag{3c}$$

$$y_0=y-\eta \tag{3d}$$

$$x_0=x-\xi \tag{3e}$$

$$\lambda=x_0-X=M(x^2+r^2)^{1/2} \tag{3f}$$

$$p=bs/U \tag{3g}$$

$$\beta^2=1-M^2 \tag{3h}$$

The function $B(p,r,X)$ in the second term in the right-hand side of Eq. (2) has an integral expression,

$$B(p,r,X)=\int_{-\infty}^{X}e^{pv}(v^2+r^2)^{-3/2}\,dv \tag{4}$$

This function can be expanded into an infinite series,

$$\begin{aligned}B(p,r,X)=&\sum_{m=0}^{\infty}U_{2m}(p,r,X)+\sum_{m=0}^{\infty}U_{2m+1}(p,r,X)\\&+\frac{p^2}{4}\sum_{n=0}^{\infty}\frac{(-1)^n}{n!(n+1)!}\left(\frac{pr}{2}\right)^{2n}\{\psi(n+1)+\psi(n+2)\}\\&-\frac{p^2}{2}\ell n\left|\frac{p}{2}\right|\sum_{n=0}^{\infty}\frac{(-1)^n}{n!(n+1)!}\left(\frac{pr}{2}\right)^{2n}\\&-i\arg[p]\frac{p^2}{2}\sum_{n=0}^{\infty}\frac{(-1)^n}{n!(n+1)!}\left(\frac{pr}{2}\right)^{2n}\end{aligned} \tag{5}$$

where $\psi(n)$ is the polygamma function with integer arguments. The terms $U_n(p,r,X)$ in the first and second summations in the right-hand side of Eq. (5) satisfy the following recursive formula:

$$U_n(p,r,X)=\frac{p^n}{(n-2)n!}\frac{X^{n-1}}{\sqrt{X^2+r^2}}-\frac{(pr)^2}{n(n-2)}U_{n-2}(p,r,X),\qquad(n\neq 2) \tag{6}$$

The initial terms to start calculations with the equation above are

$$U_0(p,r,X)=\frac{1}{\sqrt{X^2+r^2}\left(\sqrt{X^2+r^2}-X\right)} \tag{7a}$$

$$U_1(p,r,X)=-\frac{p}{\sqrt{X^2+r^2}} \tag{7b}$$

$$U_2(p,r,X)=-\frac{p^2}{2}\left\{\frac{X}{\sqrt{X^2+r^2}}+\ell n\left(\sqrt{X^2+r^2}-X\right)\right\} \tag{7c}$$

Although the integral in Eq. (4) becomes infinite when the complex argument p has a negative real part, i.e., in the left half of the p plane, the function value can be calculated by using Eq. (5), which is validated by analytic continuation.

The discretizing procedure of the integral equation follows the DPM developed for simple harmonic motion. It is straightforward to replace the harmonic kernel of the DPM with the kernel described in Eq. (2). In the ith trapezoidal element, the doublet (ξ_i,η_i) and the upwash (x_i,y_i) points are located at the one-quarter and three-quarter points on a central chord of the element, respectively. Let the area of the element be Δ_i. Then, Eq. (1) is discretized into linear algebraic equations with complex coefficients as

$$\bar{\boldsymbol{w}}=\boldsymbol{D}(p)\,\Delta\bar{\boldsymbol{p}} \tag{8}$$

where

$$\boldsymbol{D}(p)=\left[d_{ij}\right]=\left[\Delta_jK(x_i-\xi_j,y_i-\eta_j)/(8\pi)\right] \tag{9a}$$

$$\Delta\bar{\boldsymbol{p}}=\left\{\Delta\bar{p}(\xi_j,\eta_j)\right\} \tag{9b}$$

$$\bar{\boldsymbol{w}}=\left\{\bar{w}(x_i,y_i)\right\},\qquad(i,j=1,2,\ldots,N_A) \tag{9c}$$

Considering the Mangler integral, the upwash must be evaluated by the following kernel function for the upstream elements with $r<\sigma$ and $X>0$:

$$\begin{aligned}K(x_0,0)=&M^2e^{-p\lambda}/(R\lambda)+e^{-px_0}\\&\times\left\{B(p,0,-X)-\pi^2/(6\sigma^2)-p^2(\ell n\,\sigma-1)\right.\\&\left.-2\sum_{m=0}^{\infty}U_{2m}(p,0,-X)\right\},\qquad(X>0)\end{aligned} \tag{10}$$

where σ is the half-width of the element. The upwash distribution is related with wing deformation, $h(x,y,\tau)$ by

$$\bar{w}(x,y)=\frac{\partial\bar{h}(x,y)}{\partial x}+p\bar{h}(x,y) \tag{11}$$

where the overbar identifies a Laplace transform with respect to the nondimensional time, $\tau=bt/U$. Thus, the final solution of Eq. (8) becomes

$$\Delta\bar{\boldsymbol{p}}=D^{-1}(p)\left(\bar{\boldsymbol{h}}_x+p\bar{\boldsymbol{h}}\right) \tag{12}$$

where

$$\bar{\boldsymbol{h}} = \{\bar{h}(x_i, y_i)\} \tag{13a}$$

$$\bar{\boldsymbol{h}}_x = \left\{\frac{\partial \bar{h}(x_i, y_i)}{\partial x}\right\} \tag{13b}$$

If we put $p = ik$, where k is the reduced frequency of harmonic oscillation, the above procedure will coincide with the DPM in the frequency domain.

Root Loci Using the Exact Aerodynamics

The exact pressure distributions thus obtained as functions of the nondimensional Laplace variable p can be used to determine root loci of an aeroelastic system. If we adopt the expression with the generalized coordinates for the structural part, the governing equation of the system may be written as

$$\frac{1}{\omega_i^2}\ddot{q}_i + \frac{2\zeta_i}{\omega_i}\dot{q}_i + q_i = Q_i, \qquad (i = 1,2,\ldots,N) \tag{14}$$

where Q_i denotes the generalized forces. The mode shapes associated with these generalized coordinates q_i are normalized such that the coefficients of the stiffness term may become unity. In the Laplace domain, the generalized forces, Q_i can be given by

$$\bar{Q}_i = \sum_{j=1}^{N} \frac{1}{2}\rho U^2 b^3 q_{ij}(p)\bar{q}_j \tag{15}$$

where the $q_{ij}(p)$ are the unsteady aerodynamic forces associated with each generalized coordinate. Applying the Laplace transform to Eq. (14) yields

$$\frac{1}{s^2}\bar{q}_i = \sum_{j=1}^{N} A_{ij}\bar{q}_j \tag{16}$$

where

$$A_{ij} = -\delta_{ij}\left(\frac{1}{\omega_i^2} + \frac{2\zeta_i}{\omega_i p U}\right) + \frac{\rho b^5 q_{ij}(p)}{2p^2} \tag{17}$$

It should be noted here that if we put

$$\frac{1}{s^2} = -\left(\frac{1}{\omega}\right)^2(1+ig),\ p = ik, \quad \text{and} \quad \zeta_i = 0 \tag{18}$$

then Eq. (16) furnishes the conventional $U-g$ method.

The method described in the previous section, however, can provide Eq. (17) with the exact unsteady aerodynamic forces. For a given p,

$$q_{ij}(p) = \int\int_{\text{wing}} h_i(x,y)\Delta\bar{p}_j(x,y)\mathrm{d}x\mathrm{d}y \tag{19}$$

Therefore, we can solve Eq. (16) to obtain the root locus with the exact Laplace variable, $p = bs/U$. Since the forces are computed numerically, we have to resort to an iterative procedure. In the present study, the Newton-Raphson technique[9] was utilized to solve Eq. (16) in the form of a nonlinear eigenvalue problem. If we assume p, then Eq. (16) becomes virtually linear as

$$\kappa \boldsymbol{q} = \boldsymbol{A}\boldsymbol{q} \tag{20}$$

where

$$\kappa = 1/s^2 \tag{21}$$

The matrix A and the vector $\boldsymbol{q}$ in Eq. (20) are defined by the components A_{ij} in Eq. (17) and the $\bar{q}_i$ in Eq. (16), respectively. The Newton-Raphson technique combined with the linear eigenvalue solution procedure takes the following steps:

1) Assume an initial value s for the ith root at a certain speed U.

2) Calculate the corresponding nondimensional Laplace variable, $p_m = bs_m/U$ for the aerodynamics, where the subscript m denotes the mth iteration.

3) Compute each component of the matrix A.

4) Solve the complex eigenvalue problem [Eq. (20)] to obtain the eigenvalues $\kappa^{(i)}$ and their associated eigenvectors $\boldsymbol{q}^{(i)}$.

5) Choose $\kappa^{(i)}$ for tracking loci by examining the eigenvalues and eigenvectors obtained and calculate the nondimensional Laplace variable p_{m+1}.

Compare the p_{m+1} with the previous one to examine whether the convergence criterion,

$$|(p_{m+1} - p_m)/p_m| < \epsilon \tag{22}$$

is satisfied or not for a given ϵ.

7) If not, replace p_m by p_{m+1} and calculate a new p_{m+1} with the aid of the following equations to repeat the steps 3–6:

$$p_{m+1} = \{f(p_m) - f'(p_m)p_m\}/\{1 - f'(p_m)\} \tag{23}$$

where

$$f(p) = b/\{U\kappa^{(i)1/2}\} \tag{24}$$

$$f'(p) = -\frac{b}{2U}\{\kappa^{(i)}\}^{-3/2}\frac{\mathrm{d}\kappa^{(i)}}{\mathrm{d}p} \tag{25}$$

8) Continue the above procedure for the next speed $U + \Delta U$, assuming an initial p_m as the converged solution p of the previous speed U. It is also possible to change the Mach numbers simultaneously according to the speed, if the consistency of the flow parameters is necessary to trace the roots.

Rectangular Wing in Incompressible Flow

An example calculation for the aerodynamics was carried out on a rectangular wing with an aspect ratio of three in incompressible flow ($M = 0$). We now consider four typical deflection modes defined by

$h_1 = 1$ (heaving)

$h_2 = 1.2(y/3)^2 - 0.2(y/3)^4$ (bending)

$h_3 = x - 1$ (pitching)

$h_4 = (x-1)\left(1.2(y/3)^2 - 0.2(y/3)^4\right)$ (torsion)

These modes correspond to those of the example in Ref. 6. Therefore, we can directly compare our results with those of Stark.

First, since there is no exact solution with the complex value p, the convergence of the present method was examined by changing the number of computational elements on the wing. The results are shown in Fig. 1. The generalized forces q_{13} with three different numbers of elements are compared as to the relative error index. This index accounts for the deviation from the base solution, which has 16 chorwise and 25 spanwise elements for the semispan. The symmetry condition has reduced the number of elements to one-half. The convergence is uniform on the entire region of the p plane. Although the relative error appears large near a particular point, $p = -0.6 + 0.2i$, it is not substantial deterioration of the solution. The aerodynamic force q_{13} itself vanishes near this point. The figure shows that the 200 elements solution can be regarded as a favorably convergent solution.

Second, the generalized forces obtained by the use of 400 elements are compared with the corresponding results of Stark. The comparison is made in Fig. 2, which shows good agreement everywhere in the plane. It is very convincing that these completely different approaches yield almost the same results, as shown here. Stark assumed that the normalized deficiency function of the indicial response can be rendered in the form,

$$\phi(\tau) = \{a/(a+\tau)\}^n \tag{26}$$

Then, the Laplace transform of the function can be obtained as

$$L[\phi(\tau)] = \frac{(-1)^n p^{n-1} a^n}{(n-1)!} e^{ap} E_i(-ap) + \frac{(-1)^n a^{n-1}}{(n-1)!} \sum_{m=0}^{n-2} p^{n-m-2}(-a)^{-m} m! \tag{27}$$

where E_i is the exponential integral function. Components of Eq. (27) are shown in Fig. 3 with $n=3$ and $a=5.5$, which Stark selected for this wing. The good approximation indicates that the deficiency function [Eq. (26)] is remarkably adequate for the finite wing in incompressible flow. It is likely that the contribution of the function $\phi(\tau)$ in Eq. (26) was substantial for this flow case. Again, it is emphasized that the present approach has no assumptions in the Laplace transform procedure.

Rectangular Wing in Compressible Flow

For the same wing, compressibility effects on the generalized forces are examined by using the 200 element solutions. The generalized forces q_{12} at three different Mach numbers of 0, 0.6, and 0.8 are depicted in Fig. 4. The results show the complicated effects of the compressibility, especially in the left halves with high Mach numbers. The undulate surface shapes at $M=0.8$ may anticipate some difficulties in the approximation of forces by using simple functions. The surfaces shown in the figure have been drawn according to the data of the function values at each mesh point. The values between the points were interpolated by spline functions. Therefore, we cannot expect accuracy in the plot between the points if the adjacent values differ greatly. In order to examine the surge at $M=0.8$, detailed computation with a finer mesh has been done on a square region with the real part of p of -0.8 to -0.4 and the imaginary part of 0.4 to 0.8. The results from the different viewpoints are shown in Fig. 5. It looks probable that an aerodynamic singularity exists in the left half of the p plane when the flow becomes high subsonic. The generalized forces computed by 200 elements at $p=-0.4+0.4i$ with $M=0.8$ are listed in Table 1.

Comparison with the Frequency Domain Approximation

A calculation is also carried out on the forces of a control surface of a 45 deg swept-back wing. The wing configuration and the aerodynamic elements used in the computation are illustrated in Fig. 6. This example was quoted from Ref. 3. Using the Padé approximation, Vepa[3] assumed the generalized force of this control surface as

$$q_{33} = 0.118p + 0.04998 - \frac{0.03816p}{p+0.8039} \tag{28}$$

Table 1 Generalized forces at $p=-0.4+0.4i$ ($M=0.8$)

(i,j)	q_{ij}	(i,j)	q_{ij}
(1,1)	$-1.6756+0.0332i$	(1,2)	$-0.5075+0.0002i$
(2,1)	$-0.5075+0.0002i$	(2,2)	$-0.2000-0.0155i$
(3,1)	$1.1984-2.1201i$	(3,2)	$0.3460-0.6394i$
(4,1)	$0.3296-0.6335i$	(4,2)	$0.1353-0.2294i$
(1,3)	$0.9375+4.1731i$	(1,4)	$0.3050+1.2675i$
(2,3)	$0.2886+1.2734i$	(2,4)	$0.0930+0.4993i$
(3,3)	$-0.6217+0.0617i$	(3,4)	$-1.8717+0.1039i$
(4,3)	$-1.8439+0.1171i$	(4,4)	$-0.6825+0.0690i$

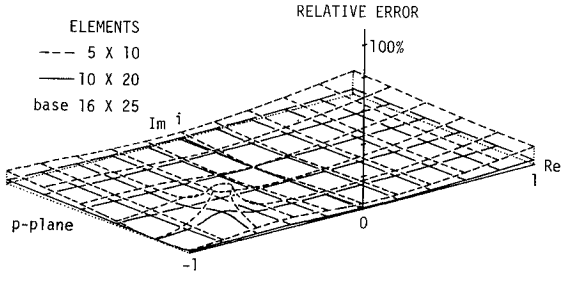

Fig. 1 Convergence of the solution.

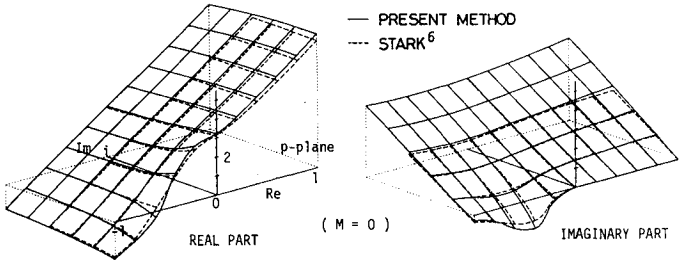

Fig. 2 Generalized force q_{13} of a rectangular wing.

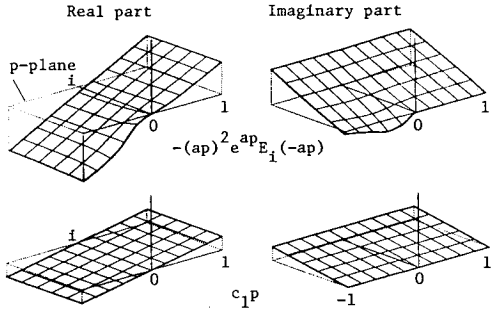

Fig. 3 Components of $L[\phi(\tau)]$, ($n=3, a=5.5$).

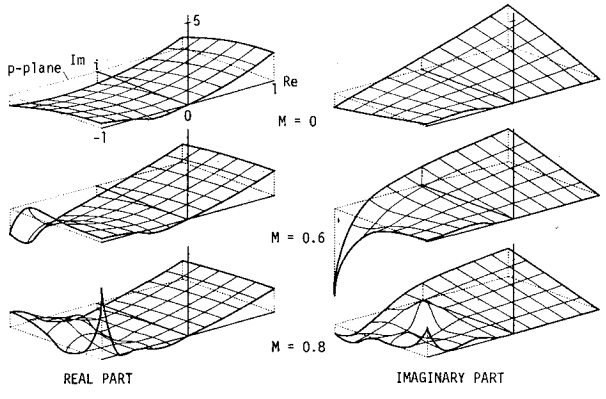

Fig. 4 Compressibility effects on q_{12}.

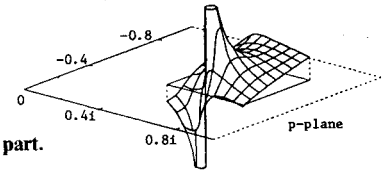

a) Real part.

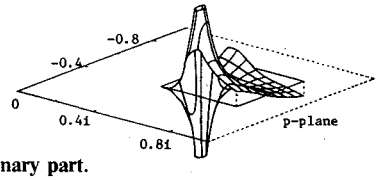

b) Imaginary part.

Fig. 5 Details of q_{12} at $M = 0.8$.

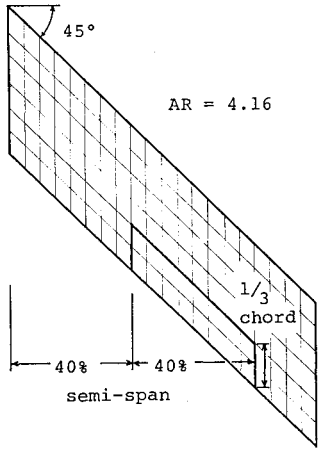

Fig. 6 Aerodynamic elements and a control surface of a swept-back wing.

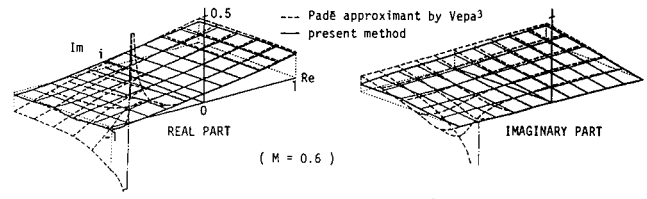

Fig. 7 Comparison on q_{33} with the Padé approximation by Vepa.

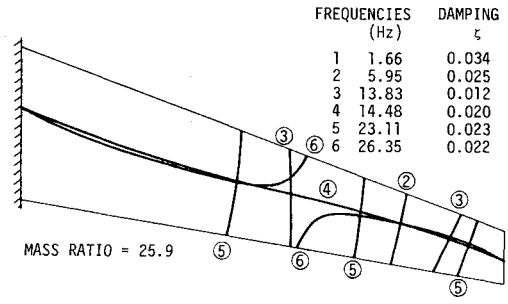

Fig. 8 Structural characteristics of a high-aspect-ratio wing.

where subscript 3 indicates the control surface deflection mode. The results of Eq. (28) are compared with those by the present method in Fig. 7. The agreement on this force is favorable in the right half-plane. However, the difference becomes appreciable as the negative real part of p increases. The singularity at $p = -0.8039$ on the negative real axis is attributed to the artificial pole of the Padé approximant in Eq. (28), whereas the present method does not bear any singularities within the range of p illustrated.

Root Loci in Incompressible Flow

Exact aerodynamic forces on the p plane have been used to determine root loci of a wind tunnel wing model. The model has a high aspect ratio, assuming an energy-efficient future transport.[10] The structural characteristics obtained for the model by the finite-element method and vibration tests are shown in Fig. 8, which illustrates natural frequencies, damping, and nodal lines of each structural mode. The root loci of this wing in incompressible flow ($M = 0$) were computed by the present method using 192 computational aerodynamical elements. The results are depicted in Fig. 9 with solid curves. Lower four modes out of the six shown in Fig. 8 were used to calculate the root loci. Numbers put near symbols in Fig. 9 indicate the flow speeds in meters per second. When the flow speed becomes zero, the four roots designated as R1–R4 coincide with the natural frequencies accompanied by viscous-type damping. As the flow speed increases up to 30 m/s, every root shows increased damping from the aerodynamic effects. The frequencies of the second and third modes, which correspond to the second and third bending modes, respectively, are almost independent of the flow speed. Meanwhile, the first bending mode (R1) and the first torsion mode (R4) approach each other as the flow speed increases. Then, the first torsion mode decreases its damping with the flow speeds over 30 m/s and penetrates the unstable region at about 37.5 m/s, i.e., the flutter speed.

The iteration procedure proposed in the analysis was proved to be effective for tracing these loci. For example, it took only four iterations for the R4 to converge at $U = 40$ m/s with an increment of 10 m/s. The error criterion [ϵ in Eq. (22)] was set to 10^{-4}. By examining the eigenvectors, no difficulty was encountered in identifying which eigenvalue could be traced, even in the case of close eigenvalues (e.g., for R3 or R4 at $U = 10$ m/s). In Fig. 9, the results for Roger's aerodynamic modeling[10] are also plotted by dashed curves. The approximation assumed the simple form with one lag term as

$$q_{ij}(p) = c_2 p^2 + c_1 p + c_0 + c_3/(p + c_4) \qquad (29)$$

in which the coefficient c_4 was fixed on 0.25 a priori. The agreement between these two results is excellent, which demonstrates a good accuracy of Roger's approximation for this flow case. For a reference, the conventional U–g curve of this wing is given in Fig. 10.

Effect of Compressibility

As the results on a rectangular wing with high Mach numbers showed a complicated variation of the aerodynamic forces in the left half of the p plane, the effects of Mach number were examined on the wind tunnel model in the root locus plane. Figure 11 illustrates the loci with four different Mach numbers. Plotting of roots R2 and R3 has been omitted for Mach 0.6 and 0.7, since the variations due to the Mach number were small. Those loci could be located between those of $M = 0$ and 0.8 for which they were traced from $U = 0$–40 m/s with the increment of 10 m/s. The loci R1 and R4 with Mach numbers of 0.6 and 0.7 have been cut below 20 m/s for the sake of simplicity. These two roots were greatly affected by compressibility. The root plunging into flutter changes from R4 to R1 between Mach 0.6 and 0.7. Furthermore, the loci changes drastically at $M = 0.8$. Despite the fact that we took into account four generalized coordinates, five roots appeared for the speeds above 15 m/s. Although we failed to track the fifth root designated as RA with speeds below 15

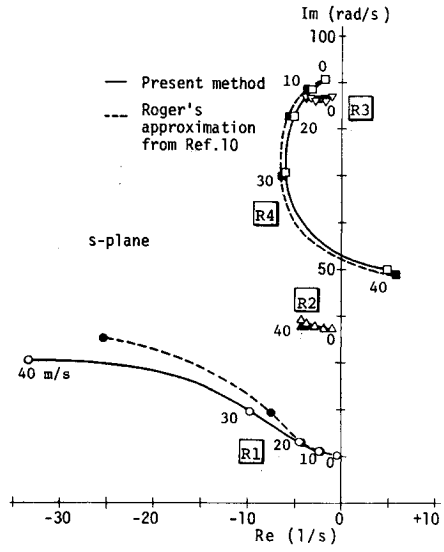

Fig. 9 Root locus with the exact aerodynamic forces ($M = 0$).

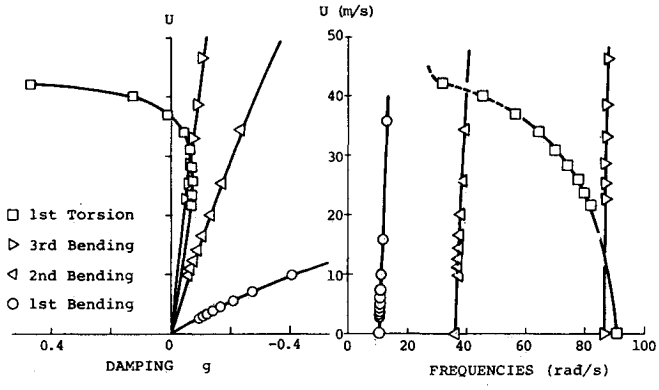

Fig. 10 Conventional $U - g$ method.

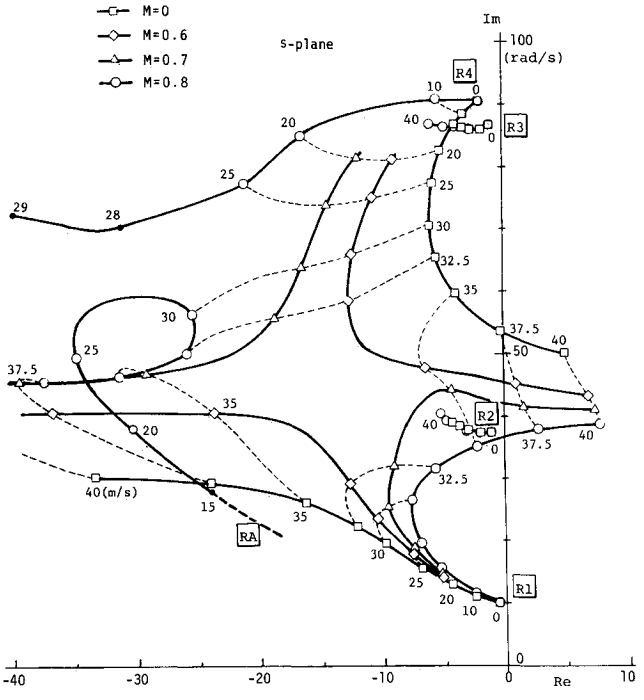

Fig. 11 Dependency of root loci on Mach numbers.

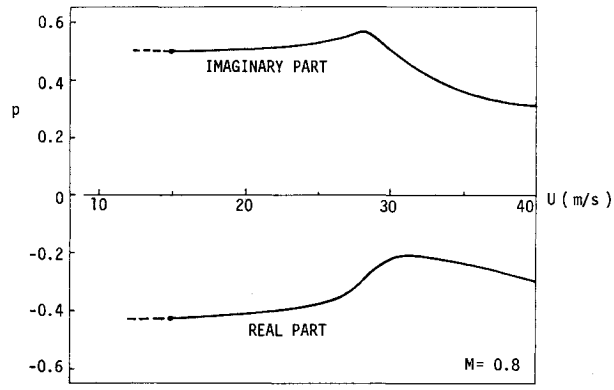

Fig. 12 Aerodynamic root as functions of p.

m/s, it may be caused by the iterative technique in Eq. (20) in which the structural roots become dominant for low flow speeds. This fact leads us to the conclusion that root RA should be an aerodynamic root. In order to confirm this, the root is replotted by the value of p vs the flow speed U. The result is shown in Fig. 12. It can be seen that the root converges to a finite value as the flow speed decreases. This behavior assures that the root is generated by aerodynamics. If the coupling between aerodynamics and structural vibrations becomes weak, the aerodynamic root should approach a certain finite value of p, since the unsteady aerodynamic forces are given as functions of p in the nondimensional form. Further, if it is the case, the aerodynamic root in the s plane approaches the origin as the flow speed becomes small.

Conclusions

A direct solution method to obtain aerodynamic forces in the so-called s plane has been developed. This solution is exact in the sense that the integral equation in the Laplace domain is numerically solved without restriction of the aerodynamic states. The kernel of the singular integral equation was exactly calculated in the left half of the s plane. The results on the generalized forces of a rectangular wing in incompressible flow demonstrated that Stark's deficiency function is adequate for that flow case. Root loci using exact aerodynamics also showed good accuracy of Roger's approximation by the finite-state modeling for incompressible flow.

Compressibility effects on the aerodynamic forces were complicated in the left half of the p plane. The surface shape of the function implies the existence of a singularity. Compressibility influences the root loci, especially the mode of coupling. In a high-subsonic case, an aerodynamic root was observed, in spite of the fact that no artificial pole had been assumed in the aerodynamics.

Acknowledgment

The author expresses his appreciation to the reviewers for their helpful suggestions regarding the manuscript.

References

[1]Ashley, H. and Boyd, W.W., "On Choosing the Best Approximations for Unsteady Potential Theory," *Küssner Anniversary Colloquium*, Göttingen, FRG, Sept. 1980, pp. 25–43.

[2]Roger, K.L., "Airplane Math Modeling Methods for Active Control Design," AGARD-CP-228, Aug. 1977.

[3]Vepa, R., "Finite State Modeling of Aeroelastic Systems," NASA CR-2779, Feb. 1977.

[4]Edwards, J.W., "Unsteady Aerodynamic Modeling and Active Aeroelastic Control," SUDAAR 504, Feb. 1977.

[5]Miyazawa, Y. and Washizu, K., "A Finite State Aerodynamic Model for a Lifting Surface in Incompressible Flow," *AIAA Journal*, Vol. 21, Feb. 1983, pp. 163–171.

[6]Stark, V.J.E., "General Equations of Motion for an Elastic Wing and Method of Solution," *AIAA Journal*, Vol. 22, Aug. 1984, pp. 1146–1153.

[7]Ueda, T. and Dowell, E.H., "A New Solution Method for Lifting Surfaces in Subsonic Flow," *AIAA Journal*, Vol. 20, March 1982, pp. 348–355.

[8]Ueda, T., "Integral Equation of Lifting Surfaces in Laplace Domain and Analytic Continuation of Its Pressure Kernel," National Aerospace Laboratory, Chofu, Japan, Rept. TR-795T, Jan. 1984.

[9]Stark, V.J.E., "A Flutter Eigenvalue Program Based on the Newton-Raphson Method," *AIAA Journal*, Vol. 22, July 1984, pp. 993–995.

[10]"Wind Tunnel Tests and Analysis on Gust Load Alleviation of a High-Aspect-Ratio Wing," ACT Study Group, National Aerospace Laboratory, Chofu, Japan, Rept. TR-890, Nov. 1985.

From the AIAA Progress in Astronautics and Aeronautics Series...

FUNDAMENTALS OF SOLID-PROPELLANT COMBUSTION – v. 90

Edited by Kenneth K. Kuo, The Pennsylvania State University
and
Martin Summerfield, Princeton Combustion Research Laboratories, Inc.

In this volume distinguished researchers treat the diverse technical disciplines of solid-propellant combustion in fifteen chapters. Each chapter presents a survey of previous work, detailed theoretical formulations and experimental methods, and experimental and theoretical results, and then interprets technological gaps and research directions. The chapters cover rocket propellants and combustion characteristics; chemistry ignition and combustion of ammonium perchlorate-based propellants; thermal behavior of RDX and HMX; chemistry of nitrate ester and nitramine propellants; solid-propellant ignition theories and experiments; flame spreading and overall ignition transient; steady-state burning of homogeneous propellants and steady-state burning of composite propellants under zero cross-flow situations; experimental observations of combustion instability; theoretical analysis of combustion instability and smokeless propellants.

For years to come, this authoritative and compendious work will be an indispensable tool for combustion scientists, chemists, and chemical engineers concerned with modern propellants, as well as for applied physicists. Its thorough coverage provides necessary background for advanced students.

Published in 1984, 891 pp., 6×9 illus. (some color plates), $60 Mem., $85 List; ISBN 0-915928-84-1

TO ORDER WRITE: Publications Order Dept., AIAA, 1633 Broadway, New York, N.Y. 10019